# Design of coupler in the near infrared incident wavelength by COMSOL

Gao Yushuang[1], Sun Jinling[2]

(1. Public Course Department, Changchun Automobile Industry Institute, Changchun 130013, China;
2. School of Economics and Management, Lanzhou University of Technology, Lanzhou 730050, China)

**Abstract:** Surface plasmon polariton (SPP) are waves that propagate along the metal-dielectric interface with exponentially decaying electromagnetic fields in both sides of the media. The strip surface plasmon waveguide has long been considered a useful device to achieve highly integrated optics. Analysis of SPP excitation and propagation characteristics in the waveguide by relying on a classic model, namely, Drude was presented. This research is conducted from visible light to near infrared incident wavelength. Strip SPP metal waveguide mode field distribution was studied. Results show that when the thickness of the metal remains constant and its width increases, the electromagnetic field distribution becomes increasingly concentrated in both sides of the strips. When the width of the strip is unchanged, thickness increases and the electromagnetic field distribution becomes increasingly focused on the metal inside. A long incident wavelength means that the concentration of metal strip around the electric field is small. Long incident wavelength can also lead to inter-channel interference. That is, having a large wavelength means one must select a wide strip waveguide. This study, which is about spontaneous radiation characteristics from 840 nm to 910 nm strip waveguide, reveals that a small part of radiation is evanescent to the metal area in the surface plasmon evanescent radiation patterns. Application design and analysis indicate that complete transfer of energy only occurs once in the limited transmission distance of the strip SPP waveguide. When the wavelength is long, the concentration field is reduced and coupling is reinforced. The designed coupler can realize optical WDM in 1 310 and 1 550 nm.

**Key words:** strip waveguide; Drude model; spontaneous radiation; optical wavelength division multiplexing

**CLC number:** O23 **Document code:** A **DOI:** 10.3788/IRLA201645.0604003

# 近红外波长下 COMSOL 软件实现新型耦合器的设计

高玉双[1],孙金岭[2]

(1. 长春汽车工业高等专科学校 公共教学部,吉林 长春 130013;
2. 兰州理工大学 经济管理学院,甘肃 兰州 730050)

**摘 要:** 一直以来条状表面等离子波导被认为是实现高集成光路的有效器件,首先采用经典的 Drude 模型对条状波导中 SPP 激发与传播特性完成了分析。针对可见光到近红外入射波长的条件完成了条

**收稿日期:**2015-10-05; **修订日期:**2015-11-03

**基金项目:**国家自然科学基金创新研究群体项目(41121001;41273010);河南省科技厅科技成果(【2014】第 2403 号)

**作者简介:**高玉双(1972-),女,副教授,硕士,主要从事计算机图形学、数据库、嵌入式系统方面的研究。Email:Double72@sina.com

状 SPP 波导的模场分布的研究,得出,当金属的厚度不变宽度越大,电磁场分布就越集中在条状波导的两侧;当金属条状的宽度不变,厚度越大时电磁场分布会越集中在金属内;入射波长越长会使得金属条状周围电场的集中越小,且还会导致信道间的干扰。利用得到的条状波导特性进而设计了一种新型的耦合器,器件设计结果表明:条状 SPP 波导在有限传输距离上能量完全转移只发生一次;波长较长时,场的集中度减小,耦合增强;条状 SPP 波导耦合器可以实现 1 310 nm 和 1 550 nm 的光波分复用。这一研究对光子器件的发展有一定的理论和实际意义。

**关键词**:条状波导; Drude 模型; 自发辐射; 光波分复用

## 0 Introduction

Surface plasmon polariton (SPP) are waves that propagate along the metal-dielectric interface with exponentially decaying electromagnetic fields in both sides of the media[1]. This unique property of SPP suggests an intriguing approach to localize and guide light in sub-wavelength metallic structures, which offers the potential to miniaturize the sizes of photonic devices into subwavelength scale[2]. Many applications based on SPP have been explored in recent years, which significantly lead to the development for high-density integration of photonic circuits[3-4]. Scientists first observed the phenomenon of surface plasmon polarization resonance in 1920 [5]. Thereafter, scientists explained the phenomenon of surface plasmon wave resonance according to surface electromagnetic wave excitation theory on the interface of metal and air[6-7]. The concept of the SPP was introduced. SPP refers to the electron density wave produced by the interaction between free vibratory electrons and incident photons exiting on the interface of the medium and metal [8-10]. Plasmon consists of charged particles, such as electrons, ions, and neutral particles (e.g., atoms, molecules, and particles). The field distribution of a surface plasmon wave has the following general features. First, the field distribution along the interface direction is highly localized. Second, the surface plasmon polarization wave, which is parallel to the direction of the interface, can be transmitted [11]. However, the surface plasmon polarization wave decreases in indexation form during the transmission process because of metal loss [12]. This rate of attenuation is very high. In the study of strip SPP waveguide, the more representative is Nezhad. It requires 1 260 $cm^{-1}$ gained compensation to achieve LRSPP nondestructive spreading in the Ag stripe membrane structure[13]; It is 10 times smaller than familiar SISPP [14]. Genov et al. utilized a semi-conducting InGaAsP silver film and found that the quality factor (Q) of the designed structure can reach up to 4 000. The gained compensation is low (approximately 200 $cm^{-1}$) when the incident wavelength is 1 400 nm. LRSPP stimulated radiation was first designed by Ambati. It is a metal striped structure of Erbium doped glass, and it can be observed in the incident wavelength of 1 532 nm. Gather et al. precisely measured the size of LRSPP spontaneous radiation in a polymer gained gold membrane structure designed at 532 nm incident wavelength [15-16]. Current studies on strip SPP waveguide mostly focus on the field of gain optimization, most of studies on the characteristics and application of strip SPP are scarce. With this background, the present research investigates the characteristics and coupler application of strip SPP by relying on the Drude model.

## 1 Propagated characteristics

Figure 1 provides a sectional view of the strip

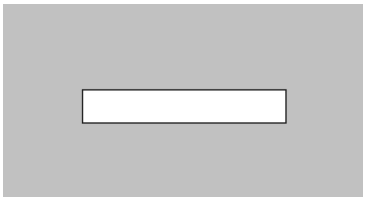

Fig.1 Strip waveguide

waveguide. The following subsections analyze the propagated characteristics of SPP in the waveguide.

### 1.1 Wave equation of SPP

In metal, conductivity is a function of frequency from the Drude model.

$$\sigma=\frac{Ne^2}{m(\gamma_D-i\varpi)}=\frac{Ne^2\gamma_D}{m(\gamma_D^2+\varpi^2)}+\mathrm{i}\frac{Ne^2\varpi}{m(\gamma_D^2+\varpi^2)} \tag{1}$$

where $m$ is electronic quality, $e$ is the electronic charge, $\gamma_D$ is the damping constant per quality with a typical magnitude order of $10^{14}\ \mathrm{s}^{-1}$. $N$ is the number of electronic per unit volume. In the optical frequency area, $\varpi$ is greater than $\gamma_D$. The imaginary part of $\sigma$ is greater than the real part, and the mental dielectric constant is:

$$\hat{\varepsilon}_{\gamma,m}=\varepsilon_\gamma+\frac{i\sigma}{\varepsilon_0\varpi}\approx\varepsilon_\gamma-\frac{Ne^2}{\varepsilon_0 m}\frac{1}{\varpi(\varpi+i\gamma_D)} \tag{2}$$

The relative dielectric constant of the metal is made up of bound electron contribution $\varepsilon_\gamma$ and free electron contribution $\frac{i\sigma}{\varepsilon_0\varpi}$. However, when $\omega$ does not approach the resonant frequency, the contribution of free electrons is greater than that of the bound electrons. Eq.(1) can then be used to replace $\varepsilon_\gamma$, and the relative dielectric constant of the metal can be written as:

$$\begin{aligned}\hat{\varepsilon}_{\gamma m}&=\varepsilon_R+j\varepsilon_I\\ \varepsilon_R&=1-\frac{Ne^2}{m(\varpi^2+\gamma_D^2)\varepsilon_0}\\ \varepsilon_I&=\frac{Ne^2\gamma_D}{m\varpi(\varpi^2+\gamma_D^2)\varepsilon_0}\end{aligned} \tag{3}$$

The above equation results in a logogram.

$$\begin{aligned}\varepsilon_R&=1-\frac{\varpi p^2}{\varpi^2+\gamma_D^2}\\ \varepsilon_I&=\frac{\varpi_p^2\gamma_D}{\varpi(\varpi^2+\gamma_D^2)}\end{aligned} \tag{4}$$

where $\varpi_p^2\equiv\frac{Ne^2}{m\varepsilon_0}$ is the plasmon oscillation frequency, $m=9.91\times10^{-31}$ is the static quality of the electron, $N$ is the number of electrons per-unit volume, $e=1.602\times10^{-19}$ is electronic power, $\varepsilon_0=8.854\times10^{-12}$, and $\gamma_D=\frac{1}{\tau_D}$ is damping constant.

### 1.2 Electromagnetic field

An important feature of SPP is that it can produce electromagnetic resonance under the condition of coupling and convert the electromagnetic energy into energy of SPP. Owing to this property, SPP can only be coupled with TM($p$) wave instead of $a$TE($s$) wave. To understand SPP transmission, one must analyze the relationship between wave vectors. In the rectangular coordinate system, we set the dependencies for harmonic electromagnetic wave and time as $\partial/\partial t=-j\omega$. The $x$-axis represents the harmonic electromagnetic wave propagated directions, and the system in the $y$-axis is constant. The Maxwell′s equations of TE and TM in air are as follows:

$$\begin{aligned}&(\mathrm{TE})\begin{cases}\dfrac{\partial H}{\partial z}-jkH_z=-j\omega\varepsilon_0\varepsilon E_y\\ \dfrac{\partial E_y}{\partial z}=-j\omega\mu_0 H_x\\ jkE_y=j\omega\mu_0 H_z\end{cases}\\ &(\mathrm{TM})\begin{cases}\dfrac{\partial E_x}{\partial z}-jkE_z=j\omega\mu_0 H_y\\ \dfrac{\partial H_y}{\partial z}=j\omega\varepsilon_0\varepsilon E_x\\ jkH_y=-j\omega\varepsilon_0\varepsilon E_z\end{cases}\end{aligned} \tag{5}$$

where $\varepsilon_0$ is the vacuum dielectric constant, $\varepsilon$ is the dielectric relative dielectric constant, $\mu_0$ is the vacuum magnetic permeability, and $k$ is the wave vector (electromagnetic waves along the direction of propagation). The following investigation is about answer to bounding on the surface of spreading TM mode field. Using Eq.(5) in the half space can result in:

$$\begin{aligned}&z>0\begin{cases}H_y(z)=A_2e^{jkx}e^{-k_2z}\\ E_x(z)=jA_2\dfrac{1}{\omega\varepsilon_0\varepsilon_2}k_2e^{jkx}e^{-k_2z}\\ E_z(z)=-A_2\dfrac{k}{\omega\varepsilon_0\varepsilon_2}e^{jkx}e^{-k_2z}\end{cases}\\ &z<0\begin{cases}H_y(z)=A_1e^{jkx}e^{k_1z}\\ E_x(z)=-jA_1\dfrac{1}{\omega\varepsilon_0\varepsilon_2}k_1e^{jkx}e^{k_1z}\\ E_z(z)=-A_1\dfrac{k}{\omega\varepsilon_0\varepsilon_2}e^{jkx}e^{k_1z}\end{cases}\end{aligned} \tag{6}$$

where $k_1$ and $k_2$ represent the wave vector, which is vertical to the interface ($z$ axis) in two types of materials. Their reciprocals, $z_{1,2}=1/|2k_{1,2}|$, define the

penetrating distance when the electromagnetic field intensity decreases to $e^{-1}$ along vertical direction within two substances, namely, metal and medium skin depth. The physical parameters further quantify the bondage degree of electromagnetic field on the material surface. The electromagnetic waves in the metal and medium skin depth are:

$$z_1=\frac{1}{k_0}\sqrt{\left|\frac{\varepsilon_1+\varepsilon_2}{\varepsilon_1^2}\right|} \text{ and } z_2=\frac{1}{k_0}\sqrt{\left|\frac{\varepsilon_1+\varepsilon_2}{\varepsilon_2^2}\right|},$$

where $k_0=2\pi/\lambda$ is the free space wave vector. The successional requirements when $H_y$ and $\varepsilon_i E_z$ is on the interface are:

$$\frac{k_2}{k_1}=-\frac{\varepsilon_2}{\varepsilon_1} \tag{7}$$

According to the index sign of the traditional definition in Eq.(7), $k_1$ and $k_2$ must be greater than zero. If $\varepsilon_2>0$, then $\mathrm{Re}[\varepsilon_1]<0$. The surface wave exists only in one condition: the real material dielectric constant component on both sides of the interface must have opposite signs. By clearing up the second and third types in the TM mode equations of Eq.(6) and then substituting the $E_x$ $E_z$ equations into the first type, the obtained $H_y$ should satisfy the wave equated expression:

$$\frac{\partial^2 H_y}{\partial z^2}+(k_0^2\varepsilon-k^2)H_y=0 \tag{8}$$

Substituting expression $H_y$ in Eq.(7) into the above equation results in $k_1^2=k^2-k_0^2\varepsilon_1$ and $k_2^2=k^2-k_0^2\varepsilon_2$. Combining the two equations yields the dispersion relations; the SPP wave spreads on the interface.

$$k=k_0\sqrt{\frac{\varepsilon_1\varepsilon_2}{\varepsilon_1+\varepsilon_2}} \tag{9}$$

Expression is applied to any $\varepsilon_1$ value (whether real or imaginary, that is, whether the electromagnetic wave is attenuating or not). It is applicable in conductor circles constantly. For the incident TE model electromagnetic wave, the expressions of electromagnetic field can be written as follows:

$$z>0\begin{cases}H_y(z)=A_2e^{jkx}e^{-k_2z}\\ E_x(z)=jA_2\dfrac{1}{\omega\varepsilon_0\varepsilon_2}k_2e^{jkx}e^{-k_2z}\\ E_z(z)=-A_2\dfrac{k}{\omega\varepsilon_0\varepsilon_2}e^{jkx}e^{-k_2z}\end{cases}$$

$$z<0\begin{cases}H_y(z)=A_1e^{jkx}e^{k_1z}\\ E_x(z)=-jA_1\dfrac{1}{\omega\varepsilon_0\varepsilon_2}k_1e^{jkx}e^{k_1z}\\ E_z(z)=-A_1\dfrac{k}{\omega\varepsilon_0\varepsilon_2}e^{jkx}e^{k_1z}\end{cases}$$

The continuity of field components in the boundary surface of $E_y$ and $H_z$ indicates that $A_1(k_1+k_2)=0$. Given that producing the surface electromagnetic wave requires $\mathrm{Re}[k_1]>0$ and $\mathrm{Re}[k_2]>0$, the requirements can be met only at the condition of $A_1=0$, namely, $A_2=A_1=0$. This condition means that under the lighting of TE polarized irradiation, the intersurface of the metal and medium will not stimulate a boundary surface wave or that the SPP wave can only be generated under the condition of TM polarized light.

## 2 Field distribution simulation

### 2.1 Field distribution

When setting the light wavelength of the excited signal in free space, $\lambda_0=0.63$ μm. The relative dielectric constant of the surrounding medium material is $\varepsilon_{\gamma,I}=2.6$. The relative dielectric constant of the metal belt is $\varepsilon_{\gamma,m}=-19-j0.53$. The $SS_b^0$ mode field distribution in the optical waveguide of the metal belt obtained through COMSOL analysis is shown in Fig.2.

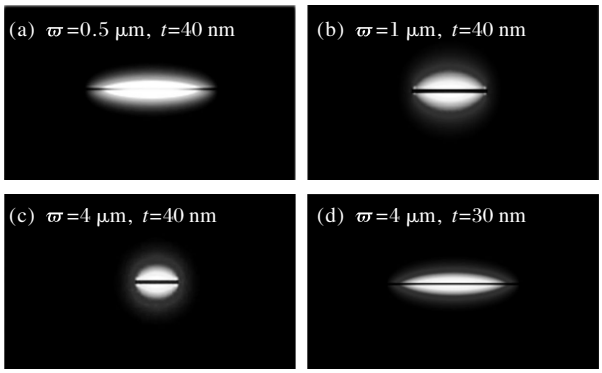


Fig.2 Metal strip waveguide mode field distribution

The figure shows that when the thickness of the metal strip (Ag) $t$ remains invariant, the width of $\omega$ increases, and the field distribution becomes concentrated on both sides of the metal belt up and down. When the width of the metal belt $\omega$ is

unchanged, its thickness increases, and the field distribution becomes concentrated because when $t$ is large, more field distribution exists in metal. Next, we need to consider how to select the parameters of the metal belt when the wavelength of light irradiation is the same. Figure 2 presents the mode field distribution of the metal belt in the case of different wavelengths.

Figure 3 shows the mode field distribution of the metal strip waveguide in the case of different wavelengths. Analysis of Fig.3 shows that when the width of the metal belt decreases, the increase in working wavelength reduces the concentration degree of the electric field around the metal band. This condition will cause interference between the channels; therefore, when the wavelength is large, a wide band should be selected.

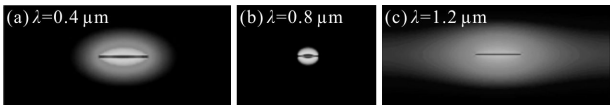


Fig.3 Different wavelengths metal strip waveguide mode field distribution

### 2.2 ASE intensity

Figure 4 shows the strip waveguide spontaneous radiation spectrum of three different amplified lengths of $l_a$ under the condition of 840 nm ≤ λ ≤ 910 nm. When the magnified area reaches the full width at half maximum of 8 nm, $l_a$=l (narrow width) and the

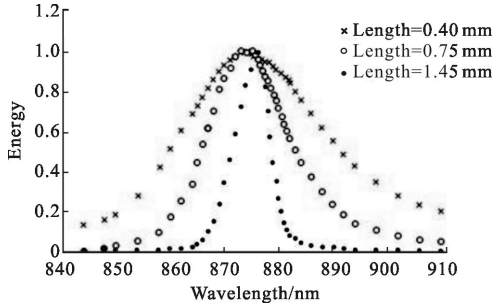


Fig.4 Three different enlarged areas of length SPP

spectrum becomes narrow. ASE in the central area is characterized by an obvious downward trend in intensity, and the structure reveals that the area is the metal strip. With anti-embrittlement state loss, most of tradiation from strip waveguide area is evanescent to the metal area. A small amount of radiation in the radiation mode of the surface plasmons is also evanescent to the metal area.

## 3 Coupler of design

The symmetric design of the coupler is shown in Fig.5. The coupler is then applied to the Ag strip structure, the width and thickness of which are 8 μm and 50 nm, under the two wavelengths of λ=1 330 nm and λ=1 550 nm (coupler operating characteristics).

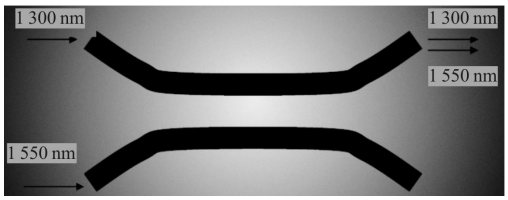


Fig.5 Schematic diagram of a wavelength division multiplexer

When λ=1 550 nm, according to $\varepsilon_{r,m}=-105.34+10.42i$, the normalized propagated constant is calculated to obtain $\frac{\beta}{\kappa_0}=1.625+i6.37\times10^{-5}$. The field distribution is shown in Fig.6 (a). When λ=1 300 nm, according to $\varepsilon_{r,m}=-75.17+6.32i$, the normalized propagated constant is calculated to obtain $\frac{\beta}{\kappa_0}=1.619+i7.53\times10^{-5}$. The field distribution is shown in Fig.6(b). Assuming that the light energy inputted directly from coupler port 1 and port 2 does not provide any input and by selecting the directed coupler length of 114 μm, the power distribution of two waveguides in two different coupler wavelengths can be obtained, as shown in Fig.6(a) and 6(b). If two types of optical signals are inputted from port 1, the inputted wavelengths are λ= 1 300 nm and λ=1 550 nm. After the direct coupler, the optical signal whose wavelength is λ=1 300 nm is outputted from port 3. The optical signal whose wavelength is λ=1 550 nm, is outputted from port 4. The light wave decomposed multiplexer and the symmetry of the directed coupler can then be determined. If the optical signals whose wavelengths are λ=1 300 nm and λ=1 550 nm respectively enter

from ports 1 and 2 into the directed coupler(length of 114 μm) and if both light signals are outputted from port 1, the function of this is light wavelength division multiplexer.

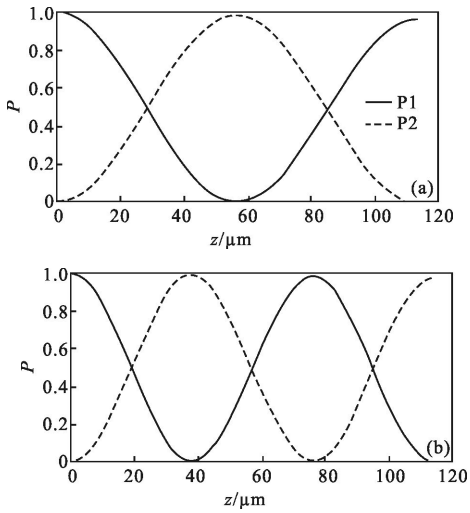


Fig.6 Light wavelength

## 4 Conclusion

The wave equation and dielectric constant in the metal strip waveguide were expanded in this study through formula deduction. The plasmon transmitted characteristics were introduced on the surface of the metal belt in detail, and analogue simulation was conducted by using the software COMSOL. When the thickness of the metal strip is invariant, the width of $\omega$ increases and the field distribution becomes increasingly concentrated on both sides of the metal belt (up and down). When the width of the metal belt $\omega$ is unchanged, its thickness $t$ increases and the field distribution becomes increasingly concentrated. Its influence (i.e., change in wavelength to surface plasmons) was also investigated. In conclusion, the increase in working wavelength reduces the concentration degree of the electric field around the metal band. This condition, in turn, causes interference between channels. Therefore, when wavelength is large, a wide band should be selected.

**References:**

[1] Hamed S M S, Eftekhar A A, Atabaki A H, et al. Band-edge bilayer plasmonic nanostructure for surface enhanced raman spectroscopy[J]. ***Eprint Arxiv***, 2014, 3(1): 66-72.

[2] Peiwen Meng, Kiyotoshi Yasumoto, Yunfei Liu. Surface plasmon resonant scattering in metal-coated dielectric nanocylinders[J]. ***Optics Communications***, 2014, 332(4): 18-24.

[3] Ye Shuji, Luo Yi. Advanced experimental methods toward understanding biophysicochemical interactions of interfacial biomolecules by using sum frequency generation vibrational spectroscopy[J]. ***Science China***, 2014, 57(12): 1646-1661.

[4] Li Zhiquan, Yan Lei, Guo Jialiang, et al. Characteristic analysis of noise factor in the periodic stripe long range surface plasmon polaritons structure [J]. ***Acta Photonica Sinica***, 2015, 44(3): 319001-0319001.

[5] Ye Shuji, Luo Yi. Advanced experimental methods toward understanding biophysicochemical interactions of interfacial biomolecules by using sum frequency generation vibrational spectroscopy[J]. ***Science China***, 2014, 57(12):1646-1661.

[6] Zheng Gaige, Xu Linhua, Chen Yunyun, et al. Beam filter and splitter based on surface plasmon propagation in ring metal heterowaveguide[J]. ***Pramana***, 2014, 83(6): 995-1002.

[7] Beltaos A, Kovacevic, Aleksander G, et al. Femtosecond laser induced periodic surface structures on multi-layer graphene [J]. ***Journal of Applied Physics***, 2014, 116(20): 204306.

[8] Lemke C, Lei08ner T, Klick A, et al. The complex dispersion relation of surface plasmon polaritons at gold/ para-hexaphenylene interfaces [J]. ***Applied Physics B Lasers & Optics***, 2014, 116(3): 585-591.

[9] Ganser A, Benner D, Waitz R, et al. Time-resolved optical measurement of thermal transport by surface plasmon polaritons in thin metal stripes [J]. ***Applied Physics Letters***, 2014, 105(19): 191119.

[10] Zhu Jun, Li Zhiquan. Analysis of characteristics with Airy surface plasmon in SPPs lasing [J]. ***Infrared and Laser Engineering***, 2014, 43(10):3298-3302.

[11] Chau Yuanfong, Hu Chihchan, Jheng Ciyao, et al. Numerical investigation of surface plasmon resonance effects on photocatalytic activities using silver nanobeads photodeposited onto a titanium dioxide layer [J]. ***Optics Communications***, 2014, 331(22): 223-228.

[12] Yang Chaojie, Zhao Huajie, Wang Peipei, et al. Polarization dependence of the light coupling to surface plasmons in an Ag nanoparticle & Ag nanowire system [J]. ***Chinese Physics B***, 2014, 23(11): 489-495.

[13] Liu C, Liu H, Zhong Y. Impact of surface plasmon polaritons and other waves on the radiation of a dipole emitter close to

a metallic nanowire antenna [J]. ***Optics Express***, 2014, 22 (21): 25539.

[14] Kekesi R, Meneses-Rodríguez D, García-Pérez F, et al. The effect of holes in the dispersion relation of propagative surface plasmon modes of nanoperforated semitransparent metallic films [J]. ***Journal of Applied Physics***, 2014, 116 (13): 134306-1-134306-5.

[15] Ahmad Naseri Taheri, Hassan Kaatuzian. Design and simulation of a nanoscale electro-plasmonic 1 ×2 switch based on asymmetric metal-insulator-metal stub filters [J]. ***Applied Optics***, 2014, 53(28): 6546-6553.

[16] Lin C H, Su C Y, Kuo Y, et al. Further reduction of efficiency droop effect by adding a lower-index dielectric interlayer in a surface plasmon coupled blue light-emitting diode with surface metal nanoparticles [J]. ***Applied Physics Letters***, 2014, 105(10): 101106.